Order in metallic glasses and icosahedral crystals

Subir Sachdev and David R. Nelson
Department of Physics, Harvard University, Cambridge, Massachusetts 02138
(Received 3 June 1985)

The relationship between short-range icosahedral order in metallic glasses and long-range order in icosahedral crystals is explored. Metallic-glass structure factors are assumed to describe liquids in metastable equilibrium just above the glass transition. A density-functional mean-field theory is then used to search for nearby crystalline states with a lower free energy. We find that undercooled liquids are metastable with respect to an icosahedral crystal, similar to the recently discovered icosahedral phase of Al-Mn. Conventional bcc and fcc crystals have an even lower free energy. The icosahedral phase is favored by the short-range icosahedral order present in the liquid. There is, however, an energetic cost associated with long-wavelength fluctuations forced in by the incommensurability of the icosahedral density waves. The theory predicts a rapid falloff of intensities in reciprocal space at small wave vectors, and a specific decoration of Penrose rhombahedra with atoms in real space. Our results are obtained via an exact mapping, in the density-functional framework, of the theory of icosahedral crystals onto the theory of conventional crystals in six dimensions.

I. INTRODUCTION

The remarkable observation by Shechtman *et al.*[1] of an aluminum-based Al-Mn alloy with long-range translational order and a perfect icosahedral point-group symmetry has stimulated a large amount of theoretical and experimental work.[2] The experimental results appear to be related to some fascinating tesselations of space originally discovered by Penrose[3] and explored in a more physical context by MacKay.[4] The three-dimensional Penrose tiling which agrees most closely with experiment has been described by Kramer and Neri,[5] and by Levine and Steinhardt.[6] Levine and Steinhardt pointed out that these tilings have δ-function Bragg peaks with an icosahedral symmetry in reciprocal space. The Fourier transform of a model which places atoms at the vertices of this Penrose lattice was subsequently obtained via an elegant projection technique by Elser,[7] Duneau and Katz,[8] and by Kalugin *et al.*[9] The exact *self-similarity* of the Penrose structures in real space should probably not be taken literally for Al-Mn; as pointed out by Elser,[10] one can locally scramble the Penrose tiles (violating the "matching rules") and still preserve the locations and δ-function character of the Bragg peaks.

Icosahedral crystals like Al-Mn appear to have both long-range orientational order and long-range translational order with an icosahedral symmetry. *Short-range* icosahedral order is believed by many investigators to be a feature of metallic glasses.[11] In this paper we explore the connection between these two different manifestations of icosahedral order.

The structural consequences of short-range icosahedral order in monatomic undercooled liquids and binary metallic glasses have recently been studied[12] using a Ginzburg-Landau theory with a uniformly frustrated order parameter.[13] An important ingredient of this theory is an unfrustrated icosahedral lattice on the surface S^3 of a four-dimensional sphere.[14–16] The lattice can be decomposed into 600 perfect tetrahedra, with particles at the vertices. The theory predicts peaks in the structure factor at positions determined by the symmetries of this ideal, curved-space icosahedral crystal. Figure 1 shows the structure factor of a relaxed dense random-packing model of metallic glasses due to Ichikawa.[17] We have labeled the peaks by the integers $n=12,20,24,\ldots$, which index reciprocal-lattice vectors in the curved-space icosahedral crystal.[13] The theory allows a good fit to structure factors of this kind, and predicts that peak positions are related by $q_{20}/q_{12}\approx 1.7$ and $q_{24}/q_{12}\approx 2.0$.[12]

Figure 2 shows that the structure factors of vapor-deposited amorphous cobalt,[18] a computer-cooled Lennard-Jones glass,[19] the bimetallic glass[20] $Mg_{70}Zn_{30}$, and the metal-metalloid glass[21] $Fe_{80}B_{20}$ have striking similarities with Fig. 1 and with each other. (For an earlier compendium of metallic-glass structure factors which makes the same point, see Ref. 11.) The $n=12$, 20, and 24 peaks present in all these structures factors are suggestive of short-range icosahedral order. The peaks are broadened relative to their sharp, curved-space counterparts, because the icosahedral order is interrupted by a dense, tangled network of wedge disclination lines.[16] Additional broadening is expected in alloys, due to compositional fluctuations (the $n=24$ peak often becomes a shoulder), and in computer-generated glasses, due to the very rapid cooling rates. Preliminary results on *glassy* Al-Mn suggests that its structure factor is qualitatively similar to those shown in Figs. 1 and 2.[22]

The frustration which prevents a simple, dense-packed lattice of perfect tetrahedra in three dimensions is often accommodated by an excess of $-72°$ disclinations. The Frank-Kasper phases[23] are *periodic* arrays of such disclination lines, with rather large unit cells.[24] Disclination lines in a predominantly tetrahedral medium are not the only means of coping with frustration, however. Face-

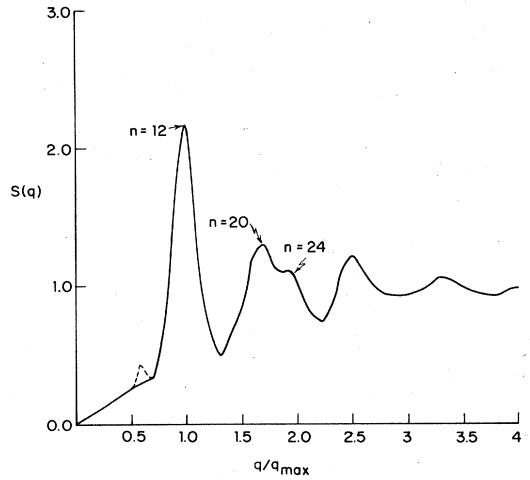

FIG. 1. Structure factor of the relaxed dense random-packing model of Ichikawa (Ref. 17). The peaks are labeled by integers $n=12,\ 20,\ 24,\ldots,$ which index reciprocal-lattice vectors characteristic of icosahedral order in a curved-space lattice of perfect tetrahedra. The dashed line is discussed in Sec. III C.

centered-cubic crystals, for example, are a 2:1 mixture of tetrahedra and *octahedra*. If one puts atoms at the vertices of a Penrose tiling, one again finds (nearly perfect) octahedra at the centers of the larger rhombahedral building blocks.[25] The parallel triangular faces of these octahedra may play a role in allowing icosahedral order in a Penrose pattern to propagate over infinite distances.

A connection between the short-range order in metallic glasses and order in icosahedral crystals is suggested by Fig. 3, which shows schematically the diffraction pattern normal to the twofold symmetry axis for icosahedral crystals. All of these Bragg peaks can be written as integer linear combinations of 12 fundamental reciprocal-lattice

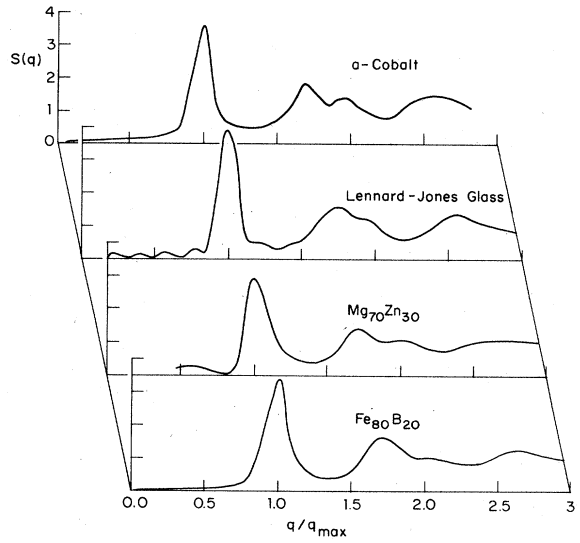

FIG. 2. Structure factors of vapor-deposited amorphous cobalt (Ref. 19), a computer-cooled Lennard-Jones glass (Ref. 20), the bimetallic glass $Mg_{70}Zn_{30}$ (Ref. 21), and the metal-metalloid glass $Fe_{80}B_{20}$ (Ref. 22). The structure factors have been rescaled to make their primary peaks coincide.

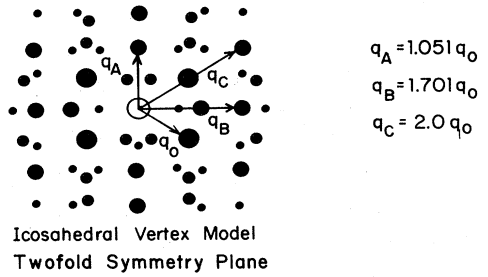

FIG. 3. Diffraction pattern for the vertex icosahedral crystal. All spots are linear combinations of a basis set of wave vectors pointing to the vertices of an icosahedron with magnitude q_0. (An alternative basis set, with magnitudes q_0/τ^3 is discussed in Sec. III D.) The wave vectors shown lie in a plane perpendicular to a twofold axis of the icosahedron. The largest spots represent members of the basis set while the smaller spots mark the positions of peaks generated by linear combinations of 2, 3, and 4 members of the basis set. q_A, q_B, and q_C are the magnitudes of wave vectors in the second generation.

vectors of length q_0 pointing to the vertices of an icosahedron.[26] Four elements of this set which lie in the twofold symmetry plane are indicated by the large dots. Smaller dots mark the positions of peaks generated by linear combinations of 2, 3, and 4 members of the basis set. As indicated in Fig. 3, there are second-generation peaks at radii which are 1.052, 1.701, and 2.0 times q_0. One might expect these peaks to be among the most intense Bragg spots. The positions of these peaks are correlated with the locations of the first three maxima in the typical metallic-glass structure factors shown in Figs. 1 and 2. The pronounced first peak in the glasses is broad enough to accommodate ordering at both the fundamental wave vector q_0 and $q_A=1.052q_0$. The $n=20$ and $n=24$ peaks are in registry with the remaining second-generation peaks at $q_B=1.701q_0$ and $q_C=2.0q_0$. These observations make it plausible that an icosahedral crystal could, under certain conditions, condense out of an undercooled liquid with structural correlations similar to those in a metallic glass.[2]

A first-principles test of this hypothesis for Al-Mn is not possible, for we do not yet know the precise locations of the aluminum and manganese atoms in the icosahedral crystal at a composition corresponding to, say, the congruent melting point. Such a study would be similar to the work of Hafner,[27] which compares the energies of metallic-glass alloys with the energies of Frank-Kasper crystals as a function of composition at $T=0$. Hafner takes into account microscopic details like electronegativity differences, valence-electron concentrations, and size ratios. He finds that, for large size ratios, Frank-Kasper phases form in alloys with minority concentrations of large atoms, and that glasses are favored with minority concentrations of smaller atoms. For other alloys, with smaller size ratios, glasses form in the same composition range as the corresponding Frank-Kasper phase.

An attractive alternative to a first-principles calculation is the density-functional mean-field theory of Ramakrishnan and Yussouff.[28] This theory examines at a mean-field level the energetic and entropic differences between the uniform liquid and ordered crystals at a given tempera-

ture. The entropy is assumed to be the entropy associated with rearranging the cells of particles with dimensions on the order of the translational correlation length. The structural energy is estimated to quadratic order in a density expansion using the structure factor of the liquid. Starting with, say, the liquid structure factor at the triple point of argon or sodium, one can make accurate, quantitative predictions about the volume, entropy, and peak intensities in the coexisting crystalline phase.[28]

Here, we use model amorphous-metal structure factors as input into the density-functional theory. These are assumed to be characteristic of undercooled liquids in metastable equilibrium just above the glass-transition temperature T_g. For simplicity we restrict our attention to one-component amorphous systems. It is not hard to generalize the density-functional approach to alloys; partial structure factors are required as input (see Sec. IV).

The density-functional approach allows us to expand the density $\rho(\mathbf{r})$ in a set of trial reciprocal-lattice vectors,

$$\rho(\mathbf{r})/\rho_0 = 1 + \sum_{\mathbf{G}} \mu_{\mathbf{G}} e^{i\mathbf{G}\cdot\mathbf{r}} , \tag{1.1}$$

and search for states with a lower free energy than the isotropic liquid. Here, ρ_0 is the mean density, and the $\{\mu_{\mathbf{G}}\}$ may be viewed as dimensionless variational parameters. In addition to reciprocal-lattice sets corresponding to bcc and fcc crystals, we also use sets with an icosahedral symmetry. There are three simple reciprocal-lattice sets which could describe icosahedral crystals, generated by stars of reciprocal-lattice vectors pointing to the vertices, edges, or faces of an icosahedron.[26] Although icosahedral crystals based on the edge or face models are always unfavorable, we find that liquids near T_g are metastable with respect to a vertex-model icosahedral crystal. fcc crystals have the lowest free energy, in accord with one's expectations for a single-component hard-sphere model. The free energy of bcc crystals is intermediate between that of a fcc lattice and that of a vertex-model icosahedral crystal. The density-functional approach allows us to predict the Bragg-peak intensities in the metastable icosahedral crystal.

The icosahedral vertex model is stabilized because the most prominent Bragg peaks are in approximate registry with the peaks in the liquid structure factor. There is, however, a special energetic cost associated with icosahedral crystals. Because the icosahedral density waves are incommensurate, one can, in principle, generate peaks everywhere in reciprocal space. There is, in particular, a penalty associated with the peaks which are generated close to the origin. This free-energy penalty is a long-wavelength manifestation of the frustration associated with icosahedral particle packings. The free energy of the icosahedral crystal is determined by a balance between this frustration and the short-range icosahedral order already present in undercooled liquids.

A number of authors have studied the stability of icosahedral crystals using truncated, phenomenological Landau expansions in the $\mu_{\mathbf{G}}$'s defined by Eq. (1.1).[29–33] Bak[30] keeps a single shell of reciprocal-lattice vectors, and appeals to fifth-order terms in the expansion to stabilize an icosahedral crystal. Mermin and Troian,[31] and Kalugin *et al.*[32] achieve stability by introducing two shells of wave vectors and truncating at fourth order. An interesting variant of these ideas has been suggested by Jaric,[33] who argues that the ordering is driven by a bond orientational order parameter whose coupling to the translational degrees of freedom causes the material to crystallize.

As emphasized by Baym *et al.*,[34] truncated Landau theories of crystallization have predictive value only when one is dealing with *weakly*-first-order phase transitions. The transition to icosahedral Al-Mn, however, is similar in many respects to ordinary crystallization,[1] which is *strongly* first order. There are, moreover, unavoidable *ad hoc* assumptions in the signs and magnitudes of expansion coefficients in the Landau approach. The density-functional mean-field theory is equivalent to carrying out a Landau expansion to all orders with known coefficients. It is straightforward to incorporate additional shells in reciprocal space. We find that around 100 shells, not just one or two, are necessary to obtain accurate free energies for the icosahedral crystal. Although there are inherent limitations in any mean-field approximation, we think the density-functional approach represents a significant improvement over the phenomenological Landau theories.

An important tool in the application of the density-functional theory to icosahedral crystals is a theorem we prove in Sec. III: The density-functional theory of an incommensurate icosahedral crystal is identical to the density-functional theory of a periodic crystal in six dimensions with a point group isomorphic to the icosahedral point group Y and a suitably chosen liquid structure factor. Similar theorems have been used to simplify Landau theories and to calculate Fourier transforms of Penrose patterns.[8–10,30,32] Our variational ansatz for the free energy amounts to specifying a particular distribution of density contours on a six-dimensional hypercubical lattice. Bak has reformulated Landau theory in this way.[30] The calculations are also closely related to Penrose tilings,[3–9] in the sense that they lead to Penrose rhombahedra, which are all decorated in approximately the same fashion [see Fig. 7(b)]. We also show that the intensity $I_{\mathbf{G}}$ of a Bragg peak in an icosahedral crystal at finite temperature is given, to an excellent approximation, by

$$\begin{aligned} I_{\mathbf{G}} &= \rho_0^2 \langle |\mu_{\mathbf{G}}|^2 \rangle \\ &= I_0 \exp(-aG^2)\exp(-bG_\perp^2) . \end{aligned} \tag{1.2}$$

The constants I_0, a, and b are determined by the structure factor of the undercooled liquid. The first exponential term in Eq. (1.2) is the usual Debye-Waller factor. The quantity $\mathbf{G}_\perp$ in the last term is a vector perpendicular to $\mathbf{G}$ in the six-dimensional (6D) space which, when added to $\mathbf{G}$, gives a reciprocal-lattice vector of the 6D crystal (see Sec. III). The main effect of the last term in (1.2) is to damp out strongly the intensities of "exotic" Bragg peaks, such as those near the origin. Elser has obtained a term like this by randomly scrambling the tiles of a Penrose lattice.[10] It is easily shown that a form like Eq. (1.2) also follows from the continuum elastic approaches of Refs. 9, 30, and 35, with a and b expressed in terms of elastic constants.

In Sec. II, we reformulate the density-functional theory

of Ramakrishnan and Yussouff in a way which can be easily generalized to icosahedral crystals. The calculations for undercooled liquids with short-range icosahedral order are described in Sec. III. The site-occupation probabilities relative to a real-space Penrose lattice are discussed in Sec. III D. The relevance of our results for icosahedral order in alloys like Al-Mn is discussed in Sec. IV.

II. DENSITY-FUNCTIONAL MEAN-FIELD THEORY

The density-functional theory of Ramakrishnan and Yussouff has been applied to understand the freezing parameters of some simple systems in both two and three dimensions.[28,36–39] The theory can be used to predict the height of the principal peak of the structure factor of the liquid when it is in equilibrium with the solid and also the change in density upon freezing. Such predictions compare favorably with experiments on fcc argon and bcc sodium. The results of the theory are also in agreement with computer experiments with hard spheres in three dimensions. The theory has recently been used in an attempt to understand hard-sphere glass transitions.[40] In this section we will present a brief discussion of the free-energy functional. For more complete derivations, see Refs. 28 and 37. We then discuss the application of this theory to freezing of conventional periodic crystals in three dimensions. Our formulation of the theory will be amenable to a simple "Gaussian" approximation, which allows us to reproduce the results of the existing calculations very simply. While this Gaussian approximation is not really necessary to minimize the free-energy functional for periodic crystals, it turns out to be essential for making the theory of incommensurate icosahedral crystals computationally tractable.

The physical idea behind the density-functional theory is the fact that at the freezing transition the translational correlation length is only a few atomic spacings. All phenomena at distances greater than the translational correlation length ξ_T can be treated in a mean-field approximation. We can imagine dividing the liquid up into cells with a dimension of the order of ξ_T centered at the points $\mathbf{r}$ with a coarse-grained local number density $\rho(\mathbf{r})$. The free energy associated with this density distribution is given by

$$\frac{F\{\rho\}}{k_B T} = \int d^3r\, \rho(r)\{\ln[\rho(r)/\rho_0]-1\} - \tfrac{1}{2}\int d^3r_1 d^3r_2\, c(\mathbf{r}_1-\mathbf{r}_2) \times[\rho(r_1)-\rho_0][\rho(r_2)-\rho_0] . \quad (2.1)$$

Here, T is the temperature and ρ_0 is the density of the uniform liquid. The first term comes from the entropy associated with dividing up the particles into the various cells. The second term is the first nonzero term in an expansion in powers of the density of the structural energy associated with variations in the density. The quantity $c(\mathbf{r})$ is the direct pair correlation function. In order that this free-energy functional give meaningful results for the spectrum of density fluctuations in the liquid, the following relation must exist between the structure factor $S(\mathbf{q})=\langle|\rho_{\mathbf{q}}|^2\rangle$ and the kernel of the second term:

$$S(\mathbf{q})=\frac{1}{1-c_{\mathbf{q}}}, \quad c_{\mathbf{q}}=\rho_0\int d^3r\, c(\mathbf{r})e^{-i\mathbf{q}\cdot\mathbf{r}} . \quad (2.2)$$

The expression for the free energy as a functional of the density can also be derived from the rigorous treatment of the static properties of classical fluids given by P. C. Martin.[41] We assume that a one-body external potential $U(\mathbf{r})$ acts on the liquid. Then the properties of the liquid with interaction Hamiltonian H can be described by the free energy W which is a functional of $U(r)$,

$$W\{u\}=\ln \mathrm{Tr}\left[\exp\left[-\beta H+\beta\int U(r)\rho_{\mathrm{mic}}(\mathbf{r})\,dr\right]\right] , \quad (2.3)$$

where $\beta=1/k_B T$ and $\rho_{\mathrm{mic}}(\mathbf{r})$ is the microscopic particle density. The physically relevant case of the grand canonical ensemble is generated when $U(r)$ is set equal to the chemical potential μ. The density in the presence of the potential is given by a functional derivative of W,

$$\frac{1}{\beta}\frac{\delta W}{\delta U(\mathbf{r})}=\langle\rho_{\mathrm{mic}}(\mathbf{r})\rangle\equiv\rho(\mathbf{r}) . \quad (2.4)$$

We now perform a Legendre transformation and focus on the quantity F, which can be shown to be a functional of ρ,

$$\beta F=\beta\int d^3r\, U(r)\rho(r)-W . \quad (2.5)$$

It is easy to show that a quadratic expansion of the free energy F in $\delta\rho(\mathbf{r})=\rho(\mathbf{r})-\rho_0$ about the ideal gas will reduce to the free-energy functional Eq. (2.1). In this formulation the relationship between $c(r)$ and $S(q)$ appears as an exact identity.

An important ingredient of the density-functional theory is the actual form assumed for the density in parameter space. If a full search of the parameter space were performed, the exact ansatz for the density would be irrelevant. Since we have to make truncations when performing the computation, it is helpful to choose an efficient ansatz. The results of Ramakrishnan and Yussouff[28] can be reproduced by an ansatz of the form

$$\frac{\rho(\mathbf{r})}{\rho_0}=\frac{1}{Z}\exp\left[\sum_{\{\mathbf{G}\}}\lambda_{\mathbf{G}}c_{\mathbf{G}}e^{i\mathbf{G}\cdot\mathbf{r}}\right] . \quad (2.6)$$

The free energy can now be expressed as a function of the parameters Z and λ_G. For positive Z, $\rho(\mathbf{r})$ is automatically positive for all real $\lambda_{\mathbf{G}}$. The Fourier-transformed pair correlation function $c_{\mathbf{G}}$ has been factored out for convenience. The vectors $\{\mathbf{G}\}$ belong to the reciprocal lattice of some Bravais lattice. By assuming this form for the density, we will by exploring the region of function space in which the density has the symmetries of the space group of the Bravais lattice. The ansatz (2.6) involves no loss of generality other than the restriction to densities which are invariant under the space group. The (dimensionless) Fourier components of the density $\mu_{\mathbf{G}}$ are defined by

$$\frac{\rho(r)}{\rho_0}=1+\sum_{\mathbf{G}}\mu_{\mathbf{G}}e^{i\mathbf{G}\cdot\mathbf{r}} , \quad (2.7)$$

which is consistent with Eq. (2.2) provided

$$\mu_{\mathbf{G}}=\frac{1}{v_c}\frac{1}{Z}\int_{v_c}d^3r\,e^{-i\mathbf{G}\cdot\mathbf{r}}\exp\left[\sum_{\mathbf{G}'}\lambda_{\mathbf{G}'}c_{\mathbf{G}'}e^{i\mathbf{G}'\cdot\mathbf{r}}\right], \quad (2.8)$$

where the integral is restricted to a unit cell of volume v_c. We assume for simplicity that the system is incompressible, in which case the constant Z is given by

$$Z=\frac{1}{v_c}\int_{v_c}d^3r\exp\left[\sum_{\mathbf{G}}\lambda_{\mathbf{G}}c_{\mathbf{G}}e^{i\mathbf{G}\cdot\mathbf{r}}\right]. \quad (2.9)$$

This should be a rather good approximation for the undercooled metallic systems of interest here. We may now insert the ansatz (2.6) into the free energy and search for a minimum in the free energy as a function of the $\lambda_{\mathbf{G}}$'s. At the minimum, the derivative of the free energy with respect to the $\lambda_{\mathbf{G}}$'s must vanish. Taking this derivative, we find that the condition for the minimization of the free energy is simply $\mu_{\mathbf{G}}=\lambda_{\mathbf{G}}$, which implies a self-consistent equation for the $\lambda_{\mathbf{G}}$'s,

$$\lambda_{\mathbf{G}}=\frac{\int_{v_c}d^3r\,e^{-i\mathbf{G}\cdot\mathbf{r}}\exp\left[\sum_{\mathbf{G}'}\lambda_{\mathbf{G}'}c_{\mathbf{G}'}e^{i\mathbf{G}'\cdot\mathbf{r}}\right]}{\int_{v_c}d^3r\exp\left[\sum_{\mathbf{G}'}\lambda_{\mathbf{G}'}c_{\mathbf{G}'}e^{i\mathbf{G}'\cdot\mathbf{r}}\right]}. \quad (2.10)$$

For simple periodic systems, it is straightforward to minimize the free energy with a given, truncated set of reciprocal-lattice vectors. For reasons discussed in Ref. 28, it is better to truncate in the $\lambda_{\mathbf{G}}$'s than in the $\mu_{\mathbf{G}}$'s. We now discuss an even simplier variational ansatz, which assumes that the real-space particle density can be written as a sum of Gaussians localized at the points of the direct-space lattice.[42] The calculations become particularly straightforward and accurate when the Gaussians have negligible overlap, so that the particles are well localized near the lattice sites of the periodic crystal. This approximation should be particularly good if the liquid and crystalline phases are separated by a sizable first-order phase transition.

To motivate the Gaussian approximation, note that according to Eq. (2.6), the density is peaked at the positions for which the argument of the exponent is maximum. This will clearly happen at coordinates $\mathbf{R}$, such that

$$e^{i\mathbf{G}\cdot\mathbf{R}}=1, \text{ for all } \mathbf{G}. \quad (2.11)$$

These positions $\mathbf{R}$ are simply the sites of the direct lattice. By expanding the argument of the exponential in Eq. (2.6) in powers of the distance from the direct lattice points, we approximate the density by a sum of Gaussians located at the vertices of the direct lattice. This amounts to replacing the ansatz (2.6) by

$$\frac{\rho(r)}{\rho_0}=\frac{\mathscr{A}}{a^3}\left[\frac{\alpha}{\pi}\right]^{3/2}\sum_{\mathbf{R}}\exp\left[-\alpha\frac{(\mathbf{r}-\mathbf{R})^2}{a^2}\right], \quad (2.12)$$

where a is the side of the conventional cubic unit cell or some other microscopic length scale for noncubic lattices. If we assume that the liquid is incompressible, the constant $\mathscr{A}$ is a function of a, given by

$$\mathscr{A}=v_c, \quad (2.13)$$

where v_c is the volume of the unit cell. Note that we replaced an infinite-parameter search for the minimum implied by the ansatz (2.6) by a two-parameter search in the variables α and a. A similar approximation appears in Refs. 40 and 42.

Given the form (2.12) for the density, it is a straightforward matter to evaluate the free energy. From Eq. (2.8) we have that

$$\mu_{\mathbf{G}}=\exp\left[-\frac{\mathbf{G}^2a^2}{4\alpha}\right]. \quad (2.14)$$

This Debye-Waller form for Fourier modes in the crystal was obtained numerically by minimizing the free energy with a large number of $\lambda_{\mathbf{G}}$'s by Haymet[39] and Ramakrishnan and Yussouff.[28] Evaluation of the entropy term in Eq. (2.1) is slightly more difficult. For *large* α, the overlaps between the Gaussians can be neglected and we obtain

$$\int d^3r\,\rho(r)\ln\left[\frac{\rho(r)}{\rho_0}\right]=\rho_0V\left\{\ln\left[\frac{\mathscr{A}}{a^3}\left[\frac{\alpha}{\pi}\right]^{3/2}\right]-\frac{3}{2}\right\}, \quad (2.15)$$

where V is the volume of the system. For *small* α, the density is almost uniform. In this case we can perform an Ewald transformation and evaluate the integral in reciprocal space. To lowest order in the fluctuation from uniform we obtain

$$\int d^3r\,\rho(r)\ln\frac{\rho(r)}{\rho_0}=\rho_0V\tfrac{1}{2}\sum_{\mathbf{G}}\exp\left[-\frac{\mathbf{G}^2a^2}{2\alpha}\right]. \quad (2.16)$$

Direct numerical calculations have shown that either the large-α expression (2.15) or the small-α expression (2.16) is a reasonable approximation over most of the range of α. In practice, the minima of the free energy always occur at α values so large that the expression (2.15) is an excellent approximation. The problem of finding the crystallike minimum in function space of the free-energy functional (2.1) has been reduced to a two-parameter minimization of the free-energy difference between the crystal and liquid given by the expression

$$\frac{\Delta F}{k_BT\rho_0V}=\ln\left[\frac{\mathscr{A}}{a^3}\left[\frac{\alpha}{\pi}\right]^{3/2}\right]-\tfrac{3}{2}-\tfrac{1}{2}\sum_{\mathbf{G}}c_{\mathbf{G}}\exp\left[-\frac{\mathbf{G}^2a^2}{2\alpha}\right]. \quad (2.17)$$

It is found that this two-parameter minimization always gives results that are within 0.2% of the more extensive calculations of Ramakrishnan and Yussouff[28] and Haymet.[39]

The theory also allows us to calculate the mean occupation number of a site of the direct lattice. Integrating the density (2.12) around the site $\mathbf{R}$, in the large-α approximation, we find for the mean occupation number of a site at $\mathbf{R}$, $\bar{n}_{\mathbf{R}}$,

$$\bar{n}_{\mathbf{R}}=\int_{\substack{v_c\\ \text{about } R}}d^3r\,\rho(r)\approx\rho_0v_c, \quad (2.18)$$

which is just the ratio of the volume per site in the crystal to the volume per particle in the liquid. This result is a consequence of the incompressibility assumption made earlier.

We close this section with some comments about the reliability of this approach. The density-functional method appears to be a good first approximation for deciding which structures are possible and isolating features of the structure factor of the liquid which are important. The theory, for instance, rules out the formation of a bcc lattice in a liquid of hard spheres at high densities, but allows its formation in the case of sodium.[28,39] Its predictions for the relative magnitudes of the order parameters for a given crystal structure are probably accurate. The theory is probably not reliable, however, for delicate questions like the energy difference between fcc and hcp crystals. Despite such limitations, we have found the density-functional approach to be surprisingly informative and predictive.

III. RESULTS FOR METALLIC GLASSES

We now explore crystalline structures which have free energies lower than those of one-component metallic glasses just above T_g. Here we view the metallic glass as a supercooled liquid with frozen-in short-range icosahedral order. The structure factor of metallic glasses is used to estimate the energetics of the short-range order in various crystalline phases, including incommensurate icosahedral crystals. Whether a given liquid actually transforms into one of these ordered phases is, of course, determined by kinetic constraints. The density-functional formalism is used to explore only the static energetics.

Only qualitative results for Al-Mn glass are available at present.[22] As a model for the short-range order in the glass we will use two structure factors: (1) the structure factor of the relaxed Bennet model of Ichikawa[18] and (2) the structure factor of vapor-deposited amorphous cobalt.[19] Although a-Co is not a glass in a conventional sense, it is believed that the same structure would form if one could cool sufficiently rapidly from the melt.[43] Amorphous cobalt is interesting because it has exceptionally sharp peaks, indicative of strong short-range icosahedral order.

A. Mapping into six dimensions

As we have pointed out in a previous paper,[26] there are three simple models for describing the density waves that might occur in an icosahedral crystal: the vertex, the edge, and the face models. We will present in detail the calculational procedure for evaluating the free-energy functional for the vertex model; the manipulations for the edge and face models are similar.

The density in the vertex model for the icosahedral crystal can be written as a sum of density waves as follows:

$$\frac{\rho(\mathbf{r})}{\rho_0}=1+\sum_{\mathbf{G}}\mu_{\mathbf{G}}e^{i\mathbf{G}\cdot\mathbf{r}}\,. \tag{3.1}$$

The vectors $\mathbf{G}$ are all integer linear combinations of a basis set of six vectors $\mathbf{g}_i$. These vectors point to the vertices of an icosahedron and can be numbered as shown in Fig. 4. A remarkable property of these six vectors is that the only way any integer linear combination of these six vectors can sum to zero is if all the integers are zero, i.e., $\sum_i n_i\mathbf{g}_i=0$, if and only if all $n_i=0$.

Because this basis set is incommensurate, the integral over the nonlinear "entropy" term in Eq. (2.1),

$$\frac{S}{k_BT}\equiv\int d^3r\,\rho(\mathbf{r})\ln\left[\frac{\rho(\mathbf{r})}{\rho_0}\right], \tag{3.2}$$

converges very slowly, which makes accurate variational calculations rather difficult. We avoid the problem of many incommensurate periodicities in the integrand by showing that (3.2) is equal to the integral over the unit cell of a conventional periodic function defined in *six* dimensions. To this end, we first map the six icosahedral basis vectors $\mathbf{g}_i$ onto six orthonormal vectors $\mathbf{g}_i^{(6)}$ in a six dimensional space. Clearly, this mapping can be extended to all the vectors in the vertex model:

$$\mathbf{G}=\sum_i n_i\mathbf{g}_i \tag{3.3}$$

maps onto

$$\mathbf{G}^{(6)}\equiv\sum_i n_i\mathbf{g}_i^{(6)}\,. \tag{3.4}$$

We also have the useful property that

$$\sum_{\{\mathbf{G}\}}\mathbf{G}=0 \tag{3.5}$$

if and only if

$$\sum_{\{\mathbf{G}^6\}}\mathbf{G}^{(6)}=0\,, \tag{3.6}$$

where $\{\mathbf{G}\}$ is any set of reciprocal-lattice vectors and $\{\mathbf{G}^{(6)}\}$ is the image of this set in the six-dimensional space. We have now established a one-to-one correspondence between the vectors in the vertex model and the reciprocal-lattice vectors of a simple hypercubic lattice in six dimensions.

With any density distribution $\rho(\mathbf{r})$, we associate a corresponding density distribution in the six-dimensional space,[30]

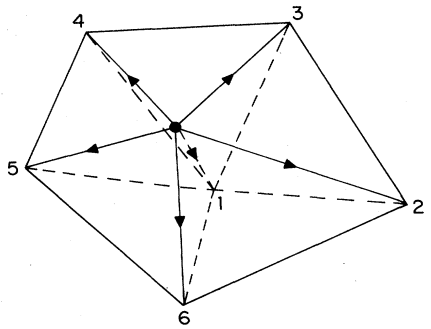

FIG. 4. Numbering convention for vectors pointing to the vertices of an icosahedron. The figure shows only the lower half of an icosahedron whose vertex is indicated by the dot.

$$\frac{\rho^{(6)}(\mathbf{x})}{\rho_0}=1+\sum_{\mathbf{G}^6}\mu_{\mathbf{G}}e^{i\mathbf{G}^{(6)}\cdot\mathbf{x}}\ . \tag{3.7}$$

The coefficients $\mu_{\mathbf{G}}$ are the same as those for the corresponding vector $\mathbf{G}$ in three dimensions, and the $\mathbf{x}$'s are six-dimensional vectors. Note that this density distribution is a conventional periodic density distribution in this six-dimensional space, with no incommensurate length scales. We now state a useful relation between integrals in three and six dimensions, namely,

$$\frac{1}{V}\int d^3\mathbf{r}\,X\left[\frac{\rho(\mathbf{r})}{\rho_0}\right]=\frac{1}{v_6}\int_{v_6}d^6\mathbf{x}\,X\left[\frac{\rho^{(6)}(\mathbf{x})}{\rho_0}\right]\ . \tag{3.8}$$

The integral in the three-dimensional space extends over the macroscopic volume V, while the integral in the six-dimensional space extends over a unit cell with volume v_6. X can be an arbitrary functional of $\rho(\mathbf{r})$. The proof of this result follows directly from (3.5) and (3.6): Insert the Fourier decompositions (3.1) and (3.7), and expand both sides of Eq. (3.8) in the $\mu_{\mathbf{G}}$'s. Since the only nonzero terms on both sides will be the ones in which the wave vectors add up to zero, the two sides are equal order by order in perturbation theory.

Another way of understanding this important result is suggested by Fig. 5. Icosahedral "quasiperiodic" functions in three dimensions can be considered as cuts through a six-dimensional periodic function.[30] In each unit hypercube that the cut intersects, a different portion of this periodic function is sampled. Since all the regions of the cube will be sampled densely, integrals over the entire cut hyperplane are equivalent to integrals over the six-dimensional unit cube.

Upon applying the identity (3.8) to Eq. (3.2), we find that the density functional for an icosahedral crystal is

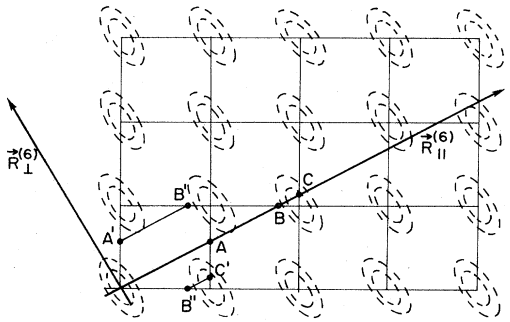

FIG. 5. Schematic illustrating how sampling a quasiperiodic function along $\mathbf{R}_\parallel^6$ is equivalent to sampling a function in a periodic function in $\mathscr{R}^{(6)}$ in a unit cell. Integrating over the segment AB is equivalent to integrating along $A'B'$, segment BC is equivalent to segment $B''C'$, etc. The elongated ovals represent contours of the density $\rho^{(6)}(\mathbf{x})$ in $\mathscr{R}^{(6)}$, as given by Eq. (3.12). Notice that even though one axis of the ovals extends across a substantial fraction of the unit cell, the overlap between them is very small.

$$\frac{F}{\rho_0 V k_B T}=\frac{1}{v_6}\int_{v_6}d^6x\,\frac{\rho^{(6)}(\mathbf{x})}{\rho_0}\left[\ln\left[\frac{\rho^{(6)}(\mathbf{x})}{\rho_0}\right]-1\right]$$
$$-\tfrac{1}{2}\sum_{\mathbf{G}^{(6)}}c_{\mathbf{G}^{(6)}}|\mu_{\mathbf{G}^{(6)}}|^2\ . \tag{3.9}$$

The second term in Eq. (2.1) has been promoted to six dimensions by going to Fourier space, replacing sums over $\{\mathbf{G}\}$ by sums over $\{\mathbf{G}^{(6)}\}$, and setting

$$c_{\mathbf{G}^{(6)}}\equiv c_{\mathbf{G}}\ . \tag{3.10}$$

We have now shown that the mean-field theory for an icosahedral crystal is equivalent to the mean-field theory of a periodic crystal in six dimensions. The function $c_{\mathbf{G}^{(6)}}$ which describes the liquid in six dimensions is a very discontinuous function of the magnitude of the reciprocal-lattice vectors in six dimensions. These discontinuities, however, do not present a significant problem in the evaluation of the free-energy functional.

B. Calculational procedure

We now analyze the density-functional theory of the periodic crystal in six dimensions. The Bravais lattice of this crystal is a simple hypercubic lattice. The point group of this lattice is not the full hypercubic group in six dimensions but a subgroup of this hypercubic group which is isomorphic to the icosahedral point group.[30] In analogy with the procedure used for ordinary crystals, we make the ansatz

$$\frac{\rho^{(6)}(x)}{\rho_0}=\frac{1}{Z_6}\exp\left[\sum_{\mathbf{G}^{(6)}}c_{\mathbf{G}}\lambda_{\mathbf{G}^{(6)}}e^{i\mathbf{G}^{(6)}\cdot\mathbf{x}}\right]\ , \tag{3.11}$$

where the $\lambda_{\mathbf{G}^{(6)}}$ are variational parameters. There is no loss in generality in this ansatz other than the restriction to densities with the translational symmetry of the hypercubic lattice and the icosahedral point group. Just as in Sec. II, we have found it a good approximation to replace this density by a sum of Gaussians located at the vertices of a hypercubic lattice in six dimensions,

$$\frac{\rho^{(6)}(\mathbf{x})}{\rho_0}=\frac{\mathscr{A}}{a^6}\left[\frac{\det Q}{\pi^6}\right]^{1/2}$$
$$\times\sum_{\mathbf{R}^{(6)}}\exp\left[-\frac{1}{a^2}(\mathbf{x}-\mathbf{R}^{(6)})_i Q_{ij}(\mathbf{x}-\mathbf{R}^{(6)})_j\right]\ , \tag{3.12}$$

where incompressibility implies that $\mathscr{A}=v_6$, the unit cell volume, and a is the side of the hypercubic unit cell. We have written the quadratic form in the argument of the exponential in terms of a general 6×6 symmetric matrix Q. This matrix cannot now be taken to be proportional to the identity because the sum of the squares of the coordinates is not the most general quadratic form invariant under the icosahedral point group.

We now use some elementary group theory to decide upon the most general form of the matrix Q. The six coordinate directions form the basis states of a six-

TABLE I. Characters for the irreducible representations of the icosahedral point group, together with characters of the representation Σ generated by the six-dimensional basis vectors discussed in the text. $\tau=(\sqrt{5}+1)/2$.

Y	E	$12C_5$	$12C_5^2$	$20C_3$	$15C_2$
A	1	1	1	1	1
F_1	3	τ	τ^{-1}	0	-1
F_2	3	τ^{-1}	τ	0	-1
G	4	-1	-1	1	0
H	5	0	0	-1	1
Σ	6	1	1	0	-2

dimensional representation Σ of the icosahedral point group. The action of the icosahedral point group upon these basis states can be simply determined from the action of the group upon the corresponding vectors in three dimensions. The character table for Σ and for all the irreducible representations of the icosahedral point group Y is shown in Table I. The number of independent quadratic forms is equal to the number of times the identity representations of Y is contained in $\Sigma\otimes\Sigma$. From Table I we determine that the identity representation occurs twice. It can be checked that the two independent quadratic invariants I_1 and I_2 are

$$I_1(\mathbf{x})=x_1^2+x_2^2+x_3^2+x_4^2+x_5^2+x_6^2 \tag{3.13a}$$

and

$$\begin{aligned} I_2(\mathbf{x})=2(&x_1x_2+x_1x_3+x_1x_4+x_1x_5+x_1x_6+x_2x_3\\ &-x_2x_4-x_2x_5+x_2x_6+x_3x_4-x_3x_5\\ &-x_3x_6+x_4x_5-x_4x_6+x_5x_6)\ . \end{aligned} \tag{3.13b}$$

It follows that the most general quadratic form in the x's is

$$\alpha' I_1(\mathbf{x})+\beta' I_2(\mathbf{x}) \tag{3.14}$$

for some constants α' and β'. The matrix Q_{ij} can now be expressed as

$$Q_{ij}=\alpha+\beta P_{ij}\ , \tag{3.15}$$

where P_{ij} is the projection matrix introduced by Elser[7]

$$P_{ij}=\frac{1}{\sqrt{20}}\begin{bmatrix} \sqrt{5} & 1 & 1 & 1 & 1 & 1\\ 1 & \sqrt{5} & 1 & -1 & -1 & 1\\ 1 & 1 & \sqrt{5} & 1 & -1 & -1\\ 1 & -1 & 1 & \sqrt{5} & 1 & -1\\ 1 & -1 & -1 & 1 & \sqrt{5} & 1\\ 1 & 1 & -1 & -1 & 1 & \sqrt{5} \end{bmatrix}, \tag{3.16}$$

with the property

$$P^2=P\ . \tag{3.17}$$

The matrix Q has two triply degenerate eigenvalues: $\alpha+\beta$ with eigenvectors lying in the three-dimensional subspace spanned by vectors of the form $P\mathbf{x}$, and the eigenvalue α with the eigenvectors lying in the three-dimensional subspace spanned by $(1-P)\mathbf{x}$. The inverse of the matrix Q is easily determined to be

$$Q_{ij}^{-1}=\frac{1}{\alpha}\left[\delta_{ij}-\frac{\beta}{\alpha+\beta}P_{ij}\right]\ . \tag{3.18}$$

The ansatz (3.12) can now be used to evaluate $\mu_{\mathbf{G}_i^{(6)}}$, with the help of the 6D generalizations of Eqs. (2.8) and (2.9). The result is

$$\mu_{\mathbf{G}_i^{(6)}}=\exp\left[-\frac{a^2}{4}G_i^{(6)}Q_{ij}^{-1}G_j^{(6)}\right]\ . \tag{3.19}$$

By some straightforward algebra we can show that this expression is equivalent to

$$\mu_{\mathbf{G}^{(6)}}=\exp\left[-\frac{a^2}{4}\left[\frac{1}{\alpha}|\mathbf{G}_\perp^{(6)}|^2+\frac{1}{\alpha+\beta}|\mathbf{G}_\parallel^{(6)}|^2\right]\right], \tag{3.20}$$

where we have defined

$$\begin{aligned} |\mathbf{G}_\parallel^{(6)}|^2&=\frac{1}{2}\left[I_1(\mathbf{G}^{(6)})+\frac{1}{\sqrt{5}}I_2(\mathbf{G}^{(6)})\right],\\ |\mathbf{G}_\perp^{(6)}|^2&=\frac{1}{2}\left[I_1(\mathbf{G}^{(6)})-\frac{1}{\sqrt{5}}I_2(\mathbf{G}^{(6)})\right]. \end{aligned} \tag{3.21}$$

$\mathbf{G}_\parallel^{(6)}$ is the projection of the vector $\mathbf{G}^{(6)}$ from the six-dimensional space along the physical three-dimensional space (see Fig. 5) and is equal to the wave vector $\mathbf{G}$. $\mathbf{G}_\perp^{(6)}$ is the projection of $\mathbf{G}^{(6)}$ along the orthogonal complement of the physical three-dimensional space.

Equation (3.20) allows us to evaluate the second term in Eq. (3.9). To evaluate the entropy, we work in the large-α and -β approximation, and neglect the overlap between Gaussians. Using the fact that $\det(Q)=\alpha^3(\alpha+\beta)^3$, we obtain

$$\begin{aligned} \frac{1}{v_6}\int_{v_6}d^6x\frac{\rho^{(6)}(\mathbf{x})}{\rho_0}\ln\frac{\rho^{(6)}(\mathbf{x})}{\rho_0}&\\ =-3+\ln\left[\frac{\mathscr{A}}{a^6}\left[\frac{(\alpha+\beta)^3\alpha^3}{\pi^6}\right]^{1/2}\right]& \end{aligned} \tag{3.22}$$

The final expression for the free-energy difference therefore reduces to

$$\frac{\Delta F(\alpha,\beta)}{k_B T \rho_0 V} = -3 + \ln\left[\frac{\mathscr{A}}{a^6}\left[\frac{\alpha^3(\alpha+\beta)^3}{\pi^6}\right]^{1/2}\right] - \frac{1}{2}\sum_{\mathbf{G}^{(6)}} c_{\mathbf{G}_i} \exp\left[-\frac{a^2}{2}\left[\frac{|\mathbf{G}_\perp^{(6)}|^2}{\alpha} + \frac{|\mathbf{G}_\parallel^{(6)}|^2}{\alpha+\beta}\right]\right] . \tag{3.23}$$

A similar analysis may be performed for edge and face icosahedral crystals. The reciprocal-lattice vectors in six dimensions that correspond to the Bragg spots in the edge model are given by[30]

$$\mathbf{G}^{(6)} = \sum_i n_i \mathbf{g}_i^{(6)} , \tag{3.24}$$

where

$$\sum_i n_i = \text{even} . \tag{3.25}$$

With an ansatz similar to (3.11), we find that a good approximation for the density is given by (3.12), where the points **R** now sit at the vertices of a bcc lattice in six dimensions. The remaining analysis for the edge model is identical to that of the vertex model.

The Bragg spots in the face model turn out to be also generated by projection from a simple hypercubic lattice in six dimensions. The fundamental set of vectors pointing to the faces of an icosahedron are given by projections of the vectors

$$\begin{aligned}
\mathbf{G}_1 &= \frac{2\pi}{a}(1,1,1,0,0,0) , \\
\mathbf{G}_2 &= \frac{2\pi}{a}(1,0,1,1,0,0) , \\
\mathbf{G}_3 &= \frac{2\pi}{a}(1,0,0,1,1,0) , \\
\mathbf{G}_4 &= \frac{2\pi}{a}(1,0,0,0,1,1) , \\
\mathbf{G}_5 &= \frac{2\pi}{a}(1,1,0,0,0,1) , \\
\mathbf{G}_6 &= \frac{2\pi}{a}(0,1,1,0,-1,0) , \\
\mathbf{G}_7 &= \frac{2\pi}{a}(0,0,1,1,0,-1) , \\
\mathbf{G}_8 &= \frac{2\pi}{a}(0,-1,0,1,1,0) , \\
\mathbf{G}_9 &= \frac{2\pi}{a}(0,0,-1,0,1,1) , \\
\mathbf{G}_{10} &= \frac{2\pi}{a}(0,1,0,-1,0,1) .
\end{aligned} \tag{3.26}$$

Because of identities like

$$\mathbf{G}_6 + \mathbf{G}_8 - \mathbf{G}_7 = \frac{2\pi}{a}(0,0,0,0,0,1) , \tag{3.27}$$

integer linear combinations of these vectors generate a hypercubic lattice. The difference between the face and vertex models now reduces simply to a difference in the values of $c_{\mathbf{G}^{(6)}}$ assigned to these reciprocal-lattice vectors. In particular, the principal peak in the structure factor now corresponds to a different wave vector in the hypercubic reciprocal lattice.

While most calculations were carred out in the approximation of Gaussians centered at the points of a Bravais lattice, a few representative calculations were carried out with the completely generaly ansatz (3.11). The integrals required for the evaluation of the free-energy functional were evaluated numerically over a six-dimensional cube. The large number of dimensions made numerical convergence of the integral a problem. The Korobov-Conroy method[44,45] for evaluating integrals over periodic functions in high-dimensional spaces was found to give the best estimates in a reasonable amount of computational time. The numerical results at the free-energy minimum were within 10% of the results obtained via the simple Gaussian approximation. Some of this discrepancy, however, is due to a lack of convergence in the numerical integration.

C. Free energies and scattering intensities

We will now present the results of the minimization of the free-energy functionals, using the structure factor of the relaxed dense random-packing model of Ichikawa[17] and the structure factor of amorphous cobolt[18] as input. With these structure factors, the energies of the fcc crystal, the bcc crystal and the vertex, edge, and face incommensurate icosahedral crystals were calculated. Table II shows the relative magnitudes and degeneracies of the first- and second-generation shells of reciprocal-lattice vectors in these models. The fcc and bcc crystals are generated from stars pointing to the faces and edges, respectively, of a regular octahedron. The differences in relative magnitude and degeneracy in Table II are, of course, the source of the different free energies of the various models.

The energies of the fcc and bcc crystals were determined from the expression (2.17). The shells of Bragg vectors are quite sparse at low wave vectors, so it is not necessary to include too many shells before we reach a region of reciprocal space where the structure factor of the liquid state is almost 1. At this point, adding additional shells has no effect on the results. About 30 reciprocal lattice vectors were required to obtain a good convergence on the energy of the crystal and magnitude of the variational parameters α and a.

The energies of the icosahedral crystals were determined by mapping the problem onto the associated six-dimensional periodic crystal and minimizing the expression (3.23). Equation (3.20) insures that we do not need to keep arbitrarily large six-dimensional reciprocal-lattice vectors **G**. About 100 shells of wave vectors in the 6D space were required to obtain convergence. In all calculations it was necessary to also minimize with respect to the overall scale parameter a.

The results of the minimization are shown in Table III. Energies are measured in units of $k_B T$. For the relaxed Ichikawa model,[17] the vertex model, the bcc and fcc crys-

TABLE II. Magnitudes and degeneracies of fundamental and second-generation shells in reciprocal space for various models.

Model	Magnitude	Degeneracy
Vertex	1	12
	1.05	30
	1.70	30
	2	20
Edge	1	30
	0.62	30
	1.18	60
	1.41	60
	1.62	30
	1.73	60
	1.90	60
	2	30
Face	1	20
	0.71	30
	1.55	30
	1.63	60
	1.87	30
	2	20
fcc	1	8
	1.15	6
	1.63	12
	1.91	24
	2	8
bcc	1	12
	1.41	6
	1.73	24
	2	12

TABLE III. Free-energy differences in units of k_BT between various ordered structures and the liquid. In (a) the structure factor of the relaxed Ichikawa model was used. The principal peak in the structure factor occurred at 3.24 Å^{-1}. Part (b) used the structure factor of amorphous cobalt with the principal peak in the structure factor at 3.20 Å^{-1}.

Model	a (Å)	α	β	ΔF
		(a)		
Vertex	1.36	21.4	420	−1.26
bcc	2.90	2090		−2.12
fcc	3.48	3540		−4.84
Edge	1.36	16.3	550	1.32
Face				
		(b)		
Vertex	1.38	13.8	281	−2.87
bcc	2.83	1443		−4.86
fcc	3.34	2371		−5.65
Edge				
Face				

tals had stable minima, while the edge model developed a local minimum with an energy higher than the liquid. The situation for amorphous cobalt was similar. The vertex model and the bcc and fcc crystals gave well-defined minima, while the edge model had only a liquidlike minimum. No ordered minimum was ever found for the face model with these structure factors.

Despite the complexity of the calculations, several enlightening and simple features can be elucidated. The parameter a took on a value such that the reciprocal-lattice stars of all stable crystalline phases were aligned with the first peak in the structure factor. Contributions from this peak tend to stabilize crystalline phases relative to the liquid. Another important feature of the structure factor is the large dip between the first two peaks. The details of how well the shells in reciprocal space avoid this dip determine the relative energies of the bcc and fcc crystals. This is essentially the reason for the fcc crystal having a lower energy than the bcc crystal. The energies of these crystals are lower for the case of amorphous cobalt because the principle peak in the liquid structure factor is much higher.

As we discussed in the Introduction, the lowest-order shells in the icosahedral vertex model match up almost perfectly with the peaks in the structure factor. This is the reason for the existence of well-defined minima for both the structure factors with density waves at wave vectors prescribed by the vertex model. Based solely upon this argument, however, one would expect that the energy of the vertex model would be lower than that of the fcc and bcc crystals. This is where the incommensurability of the icosahedral density waves in three dimensions makes an important difference. Unlike the conventional periodic crystals, the icosahedral crystals have Bragg peaks at arbitrarily small wave vectors. The structure factor of the liquid at these small wave vectors is extremely small and therefore is unfavorable to crystallization [recall that $c_{\mathbf{G}}=1-S^{-1}(\mathbf{G})$ in Eq. (3.9)]. It is the hindering influence of these low wave-vector peaks which raises the energy of the vertex model above that of the conventional crystals. In the icosahedral edge and face models, these low wave-vector peaks, together with the lack of registry of the low-order Bragg peaks with the peaks in the structure factor, are enough to destroy the stability of these phases relative to the liquid.

Knowing the strengths $\rho_{\mathbf{G}}$ of the density waves in the icosahedral vertex model allows us to predict the Bragg scattering pattern. The intensities of the Bragg peaks are proportional to $|\mu_{\mathbf{G}}|^2$. In Fig. 6 we show the spot pattern obtained using the structure factor of the relaxed Ichikawa model input, in planes which are perpendicular to the twofold, threefold and fivefold symmetry axes.

The spot patterns in reciprocal space are determined in this theory by Eq. (3.20). Its validity depends solely upon the density having a rapid falloff near the vertices of the 6D Bravais lattice. This in turn requires that the liquid be separated from the icosahedral vertex model by a sizable first-order phase transition. The structure factor then only enters to determine the values of the constants α and β. In practice we find that $\beta \gg \alpha$, so the intensity of any Bragg spot is dominated by the values of $G_\perp$ and α, except for very large $G_{||}^{(6)}=G$.

The most important factor determining α is the rate of falloff of the input structure factor at small wave vectors.

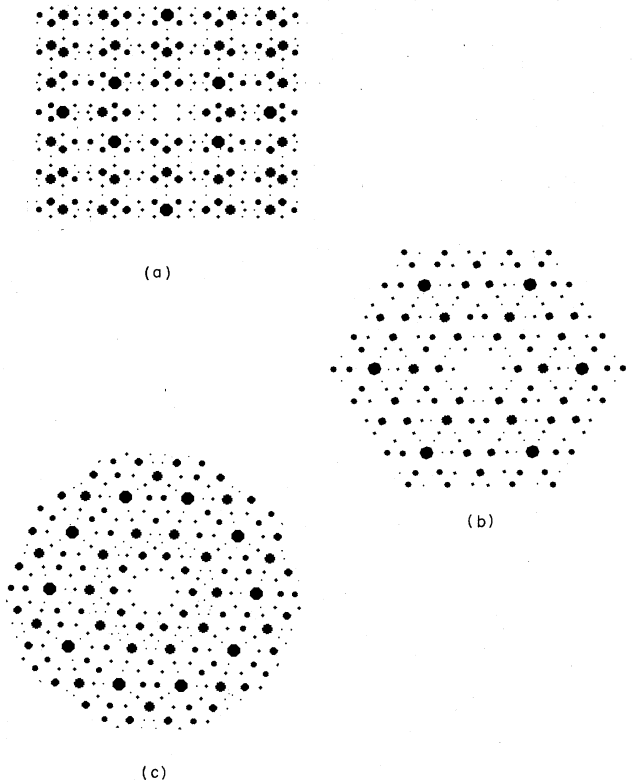

FIG. 6. Spot pattern perpendicular to the (a) twofold, (b) threefold, and (c) fivefold axes of an icosahedron. The areas of the spots represent actual intensities as predicted by the structure factor of the relaxed Ichikawa dense random-packing model (Fig. 1.).

Because the data for our input structure factors do not extend to very small wave vectors, we have used a simple two-parameter quadratic extrapolation of the structure factor to 0 at the longest wavelengths. Small changes in the structure factor at large wavelengths can produce interesting changes in the results. The original dense random-packing data of Ichikawa,[17] for example, had the small hump below the main peak indicated by the dashed line in Fig. 1. Because we were concerned about finite-size effects in Ichikawa's model, we replaced this hump by the solid curve shown in Fig. 1. If the hump is included in the calculations, the Bragg intensities change and the energy of the icosahedral vertex model is lowered to -3.31, i.e., below the energy of a bcc crystal.

Treating the α and β as adjustable constants in Eq. (3.20) may be a profitable way to parametrize experimental data. X-ray scattering measurements by Bancel *et al.*[46] on Al-Mn show a strong monotonic dependence of intensities on the value of $G_\perp$. This in turn implies that $\alpha \ll \beta$, suggesting that the small-vector density fluctuations are important in determining the stability of the phase.

D. Real-space structures

In addition to predicting the intensities of the spots in reciprocal space, the theory also yields useful information in real space. The density $\rho(\mathbf{r})$ for the crystalline bcc and fcc structures consists of sharply peaked Gaussians at the vertices of the direct lattice. The mean occupation number of a site of the lattice can be computed from Eq. (2.18). We use the values of a computed in the previous section. A rough estimate of the value of ρ_0 is contained in Ref. 17 for the Ichikawa structure, and for cobalt we use the room-temperature crystalline density. We obtain values for the mean occupation number of a site which are ≈ 1 for the bcc structure and ≈ 0.9 for the fcc structure using both structure factors. The lower mean occupation number of the fcc lattice is a consequence of its high packing fraction and of the assumption of incompressibility.

The density $\rho(\mathbf{r})$, as given in Eq. (3.1) for the vertex icosahedral crystal, has a more complicated form. It is simplest to think of this density as a three-dimensional cut along $\mathbf{R}_\parallel^{(6)}$ through a six-dimensional periodic density $\rho^{(6)}(\mathbf{x})$ lying in the space $\mathscr{R}^{(6)}$. The six-dimensional density consists of a lattice of elongated ellipsoids as shown in Fig. 5. Only those ellipsoids close to the hyperplane have a significant intersection with the three-dimensional space $\mathscr{R}_\parallel^{(6)}$. A convenient way to summarize these results is to integrate the density across the ellipsoid along $\mathbf{R}_\parallel^{(6)}$: this integral then yields the mean occupation number of a site of the icosahedral crystal. Associated with the ellipsoid at the site $\mathbf{R}^{(6)}$ in $\mathscr{R}^{(6)}$, we now have a site of the icosahedral crystal. This site occurs at the point $\mathbf{R}_\parallel^{(6)}$ which is the projection of $\mathbf{R}^{(6)}$ into $\mathscr{R}_\parallel^{(6)}$,

$$(R_\parallel^{(6)})_i = P_{ij} R_j^{(6)} . \tag{3.28}$$

From Eq. (3.12) the mean occupation number of this site can be calculated. The mean occupation number of a site at $\mathbf{R}_\parallel^{(6)}$ is

$$n(\mathbf{R}_\parallel^{(6)}) = \rho_0 a^3 \left[\frac{\alpha}{\pi}\right]^{3/2} \exp\left[-\alpha \left[\frac{\mathbf{R}_\perp^{(6)}}{a}\right]^2\right] , \tag{3.29}$$

where $|\mathbf{R}_\perp^{(6)}|$ is the distance of $\mathbf{R}^{(6)}$ from $\mathbf{R}_\parallel^{(6)}$,

$$(R_\perp^{(6)})_i = (1-P)_{ij} R_j^{(6)} . \tag{3.30}$$

Figure 7(a) depicts the mean occupation numbers of the sites $\mathbf{R}_\parallel^{(6)}$ obtained from the amorphous-cobalt calculation in a slab of thickness $\frac{1}{2}d$ oriented normal to a fivefold icosahedral symmetry axis. Here, d is the position of first peak in the radial distribution function of a-Co. It can be viewed as an effective hard-sphere diameter. Each occupied site is represented by a dot whose area is proportional to the site occupation number. In contrast to ordinary periodic crystals, there is considerable dispersion in the site occupation numbers. Some occupation numbers are larger than one, suggesting that these sites are occasionally filled with split interstitials. Clusters of sites with small occupation numbers presumably correspond to atoms which hop among various vacancy sites. Note that sites with significant occupation probability are rarely closer than the effective hard-sphere diameter d. The results from the dense-random-packing calculation are similar, except that there is more dispersion in the site occupation numbers.

Also shown in Fig. 7 are vertices of the Penrose tiling

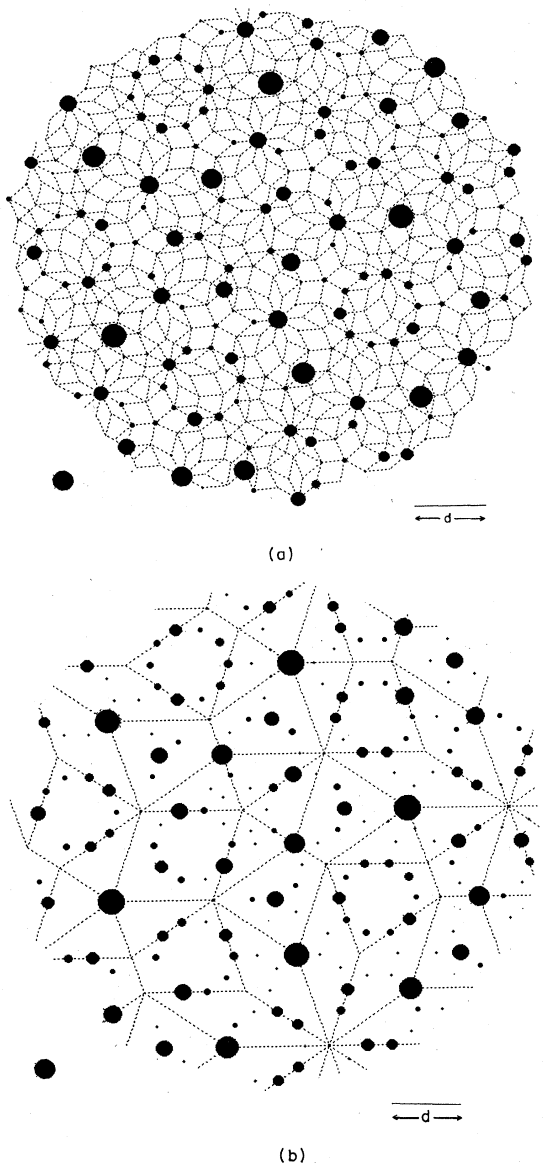

FIG. 7. (a) Sites of the vertex icosahedral crystal and the Penrose rhombohedra projected along planes perpendicular to a fivefold symmetry axis. A slice of thickness $d/2$ is taken through the real-space density. The distance d, indicated in the lower right, is an effective hard-sphere radius. The areas of the circles are proportional to the mean occupation probability of the site. The circle in the lower left has an area equivalent to a unit occupation probability. This figure was obtained from the structure factor of amorphous cobalt. (b) The same distribution of occupation numbers as in (a), but now shown relative to a Penrose lattice expanded by a factor τ^3.

obtained via Elser's projection technique from the 6D hypercubic lattice.[7] Again, only those vertices lying in a slab of thickness $d/2$ are shown. Many unoccupied vertices are projected, so this particular Penrose lattice is not a very useful way of describing the icosahedral crystal.

It is clear that a decomposition of space into larger Penrose rhombohedra is required. A remarkable property of the diffraction pattern shown in Fig. 6 is that all the spot positions remain invariant under a dilatation by a factor of τ^3, where $\tau=1.618\ldots$ is the golden mean. This τ^3 invariance becomes apparent when the diffraction pattern is viewed in a plane normal to the twofold symmetry axis. We have so far made the projection of the six-dimensional reciprocal-lattice vector $(2\pi/a)(1,0,0,0,0,0)$ line up with the first peak in the liquid structure factor. Because of the τ^3 invariance, we could equally well project elementary reciprocal-lattice vectors of the form $(2\pi/a')(1,0,0,0,0,0)$, where

$$a'=\tau^3 a \tag{3.31}$$

could be interpreted as the spacing of an expanded, six-dimensional hypercubic lattice. The first peak in the structure factor now corresponds to the projection of $(2\pi/a')(2,1,1,1,1,1)$. This transformation can be extended to all wave vectors of the icosahedral crystal. If we denote a general 6D reciprocal-lattice vector by $(2\pi/a)(n_1,\ldots,n_6)\equiv(2\pi/a)\mathbf{n}$, the identification between old and new reciprocal-lattice vectors is

$$\frac{2\pi}{a}\mathbf{n}\rightarrow\frac{2\pi}{a'}[\sqrt{20}P\mathbf{n}-(\sqrt{5}-2)\mathbf{n}]\ , \tag{3.32}$$

where P is the matrix displayed in Eq. (3.16).

After repeating the density-functional calculation with this new basis, we can obtain an expanded Penrose lattice by projecting the 6D hypercubic lattice with spacing a'. The projected particle density must, of course, be the same. It can be verified that the only changes the calculations are to replace are the variational parameters α and β, by α' and β', where

$$\alpha'=\alpha/\tau^6\ , \tag{3.33a}$$

$$\alpha'+\beta'=(\alpha+\beta)\tau^6\ . \tag{3.33b}$$

Although these transformations leave the density in the physical three-dimensional space $\mathscr{R}_{\parallel}^{(6)}$ invariant, the density in the six-dimensional space is changed. The lattice constant a has increased by a factor of τ^3. The centers of the ellipsoids are now spaced farther apart. The ellipsoids are now longer in the $\mathbf{R}_{\perp}^{(6)}$ direction by a factor of τ^3 and narrower in the $\mathbf{R}_{\parallel}^{(6)}$ direction by a factor of τ^3, these lengths being measured as fractions of the new lattice constant.

Figure 7(b) shows the same slab of particles as in Fig. 7(a), except that the site occupation numbers are now shown relative to the expanded Penrose lattice. The vertices of the expanded Penrose lattice are now shown if they are within $\tau^3 d/2$ of the center of the slab. The elementary large and small rhombahedra which make up the Penrose pattern project into a variety of four- and three-sided figures. A particularly striking feature of Fig. 7(b) is that figures with the same shape are decorated by atoms in approximately the same way. This suggests that all large and all small Penrose rhombohedra carry similar distributions of atoms.

To check this hypothesis, we have examined the site occupation numbers greater than 0.05 on the large and small Penrose rhombohedra. All the vertices of the rhombohedra have an occupation number near 1. One can describe other points of the rhombohedra as follows:[7] The triplet

of numbers (a,b,c) $(0 \leq a,b,c, \leq 1)$ corresponds to the point

$$a\hat{e}_l + b\hat{e}_m + c\hat{e}_n \ , \tag{3.34}$$

where $\hat{e}_l$, $\hat{e}_m$, and $\hat{e}_n$ are three of the six icosahedral directions. The large rhombohedron corresponds to a triplet of unit vectors such as $\{\hat{e}_1,\hat{e}_2,\hat{e}_3\}$ in Fig. 4, while the small rhombohedron corresponds to a triplet such as $\{\hat{e}_2,\hat{e}_3,\hat{e}_4\}$. The following additional sites of the large rhombohedron have a significant occupation probability, which is typically 0.5 or less:

$$\begin{aligned}&(\tau-1,\tau-1,0),\ (\tau-1,\tau-1,1),\ (2-\tau,2-\tau,0),\ (2-\tau,2-\tau,1),\ (4-2\tau,2-\tau,2-\tau)\ ,\\ &(4-2\tau,5-3\tau,5-3\tau),\ (4-2\tau,4-2\tau,4-2\tau),\ (2\tau-3,\tau-1,\tau-1)\ ,\ (2\tau-3,3\tau-4,3\tau-4)\ ,\\ &(2\tau-3,2\tau-3,2\tau-3)+\text{permutations}\ .\end{aligned} \tag{3.35}$$

Only a fraction of these sites ($\sim 20\%$) have a significant occupation probability in any given rhombohedron. The sites on the faces of the rhombohedra are, however, almost always present and are shown in Fig. 8(a). The sites of the small rhombohedron (other than vertices) which have a significant occupation are

$$(\tau-1,2-\tau,0),\ (\tau-1,2-\tau,1)+\text{permutations}\ . \tag{3.36}$$

The more prominent sites on the faces are shown in Fig. 8(b).

IV. DISCUSSION

We have shown, using a density-functional mean-field theory, that one-component undercooled liquids are metastable with respect to a vertex-model icosahedral crystal,

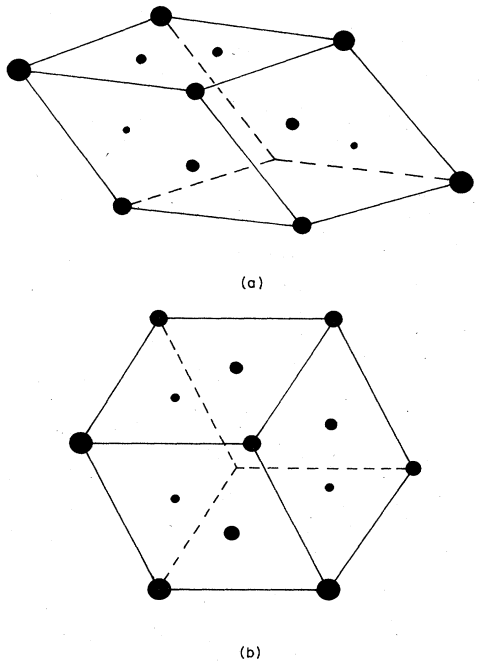

FIG. 8. (a) Typical prolate (larger) rhombohedron decorated with sites of high occupation number. The areas of the circles are proportional to the mean occupation number at the sites. Only the sites on the three faces of the rhombohedron nearest the viewer are shown. (b) The same as (a) for the oblate (smaller) rhombohedron.

similar to icosahedral Al-Mn. The calculations assume that the structure of an undercooled liquid is similar to relaxed dense-random packing. We have also used the closely related structure factor of vapor-deposited amorphous cobalt as input, because it appears to exhibit an exceptional degree of short-range icosahedral order. The stability of the icosahedral crystal is related to the short-range icosahedral order already present in an undercooled liquid.

As discussed in Sec. III D, the density-functional formalism allows us to visualize how the atoms of an icosahedral crystal are distributed in real space. If we use the particle spacing in amorphous cobalt as an effective hard-sphere diameter, the edges of the expanded Penrose rhombahedra shown in Fig. 7(b) turn out to be about 4.1 Å. This is rather close to the edge length of 4.6 Å which appears to be appropriate to icosahedral Al-Mn.[47] In their discussion of microscopic models for icosahedral Al-Mn, Elser and Henley place manganese atoms at the vertices of the Penrose rhombahedra, and put aluminum atoms at various positions on the faces and edges.[47] We too find two different classes of sites, those with occupation numbers of order unity (on the vertices), and those with smaller occupation numbers (primarily on the faces). About 30% of the atoms sit at vertex sites, suggesting that these are indeed the relevant sites for the minority atoms (manganese) in Al-Mn alloys. Icosahedral Al-Mn forms in a composition range of about 10 to 25% manganese.[48] The fraction of atoms sitting at the vertices in our calculation would be lowered from 30% to this range by a small change in the parameter α. The many small occupation numbers we find away from the vertices of the Penrose lattice suggest that, if we associate aluminum atoms with these sites, they are disordered, like the mobile phase in a superionic conductor.

To check these conclusions, one must repeat these calculations for two-component alloys. As we have seen in Sec. III C, the addition of a "prepeak" in the structure factor such as that shown by the dashed line in Fig. 1 lowers the free energy relative to conventional periodic crystals. It is interesting to note that prepeaks do in fact occur in two-component metallic glasses with a high degree of chemical short-range order.[49]

The extension of the Ramakrishnan-Yussouff formalism to two-component liquids is straightforward: if $\rho_A(\mathbf{r})$ and $\rho_a(\mathbf{r})$ are the coarse-grained number densities of the two components, the free-energy functional is

$$\frac{F[\rho_A,\rho_B]}{k_BT}=\int d^3r\left[\rho_A(\mathbf{r})\ln\frac{\rho_A(\mathbf{r})}{\rho_{A,0}}-1\right]+\int d^3r\left[\rho_A(\mathbf{r})\ln\frac{\rho_B(\mathbf{r})}{\rho_{B,0}}-1\right]$$

$$-\tfrac{1}{2}\int d^3r_1\int d\mathbf{r}_2[\,C_{AA}(\mathbf{r}_1-\mathbf{r}_2)\delta\rho_A(\mathbf{r}_1)\delta\rho_A(\mathbf{r}_2)+2C_{AB}(\mathbf{r}_1-\mathbf{r}_2)\delta\rho_A(\mathbf{r}_1)\delta\rho_B(\mathbf{r}_2)+C_{BB}(\mathbf{r}_1-\mathbf{r}_2)\delta\rho_B(\mathbf{r}_1)\delta\rho_B(\mathbf{r}_2)]\,, \quad (4.1)$$

where $\rho_{A,0}$ and $\rho_{B,0}$ are the densities in the uniform liquid and

$$\delta\rho_A(\mathbf{r})=\rho_A(\mathbf{r})-\rho_{A,0}\,, \quad (4.2a)$$

$$\delta\rho_B(\mathbf{r})=\rho_B(\mathbf{r})-\rho_{B,0}\,. \quad (4.2b)$$

The first term comes from the entropy of an ideal binary mixture.[50] The partial direct correlation functions in the remaining terms require knowledge of the partial structure factors in the liquid. These are related to the total x-ray scattering intensity $I(q)$ in the liquid by

$$I(q)=Z_a^2S_{AA}(\mathbf{q})+2Z_aZ_bS_{AB}(q)+Z_b^2S_{BB}(\mathbf{q})\,, \quad (4.3)$$

where Z_a and Z_b determine how strongly x rays scatter from the different species.

Ideally, one would like to use partial structure factors extracted from careful experiments on glassy Al-Mn as input into the calculations. If these were unavailable, an attractive alternative would be to use a computer-generated, relaxed two-component dense random-packing model, with sphere diameters in a ratio appropriate to aluminum and manganese. Excellent fits to the structure factors of metallic glasses can be obtained by this method.[51]

Notes added in proof. (1) After this paper was submitted for publication, we were informed of density-functional calculations by Haymet and co-workers,[52] who use structure factors appropriate to liquids near the melting point as input. No icosahedral phase was found, presumably because liquids near the melting point possess only a modest amount of short-range icosahedral order.

(2) Recently, Poon *et al.*[53] have reported the discovery of an amorphous metallic glass alloy with approximate composition $Pd_{60}U_{20}Si_{20}$ which transforms into an icosahedral crystal upon annealing. This experiment lends support to the close connection between order in metallic glasses and icosahedral crystals enunciated in this paper.

ACKNOWLEDGMENTS

It is a pleasure to acknowledge helpful conversations with J. Hafner, B. I. Halperin, D. Shechtman, F. Spaepen, and D. Turnbull. We are particularly indebted to C. Henley for explaining the results of Ref. 47 to us, and for suggesting that we scale up our Penrose lattice by τ^3. This work was supported by the National Science Foundation, through the Harvard Materials Science Laboratory and through Grant No. DMR-82-07431.

[1]D. Shechtman, I. Blech, G. Gratias, and J. W. Cahn, Phys. Rev. Lett. **53**, 1951 (1984).
[2]For a review, see D. R. Nelson and B. I. Halperin, Science **229**, 233 (1985).
[3]R. Penrose, Bull. Inst. Maths. Appl. **10**, 7/8, 266 (1974); see also M. Gardner, Sci. Am. **236**, 110 (1977).
[4]A. L. MacKay, Physica **114A**, 609 (1982); see also A. L. MacKay, Kristallografiya **26**, 910 (1981) [Sov. Phys.—Crystallogr. **26**, 517 (1981)].
[5]P. Kramer and R. Neri, Acta Crystallogr. Sect. A **40**, 580 (1984).
[6]D. Levine and P. J. Steinhardt, Phys. Rev. Lett. **53**, 2477 (1984).
[7]V. Elser, Acta Crystallogr. Sect. A (to be published).
[8]M. Duneau and A. Katz, Phys. Rev. Lett. **54**, 2688 (1985).
[9]P. A. Kalugin, A. Yu Kitaev, and L. C. Levitov, J. Phys. (Paris) Lett. **46**, L601 (1985).
[10]V. Elser, Phys. Rev. Lett. **54**, 1730 (1985).
[11]See, e.g., C. L. Briant, Discuss. Faraday Soc. **61**, 25 (1976).
[12]S. Sachdev and D. R. Nelson, Phys. Rev. Lett. **53**, 1947 (1984); Phys. Rev. B **32**, 1480 (1985).
[13]D. R. Nelson and M. Widom, Nucl. Phys. B **240** [FS12], 113 (1984).
[14]H. S. M. Coxeter, Ill. J. Math. **2**, 746 (1958); see also H. S. M. Coxeter, *Introduction to Geometry* (Wiley, New York, 1969).
[15]J. F. Sadoc, J. Phys. (Paris) Colloq. **41**, C8-326 (1980); see also J. F. Sadoc, J. Phys. (Paris) Lett. **44**, L707 (1983).
[16]D. R. Nelson, Phys. Rev. Lett. **50**, 982 (1983); Phys. Rev. B **28**, 5515 (1983).
[17]T. Ichikawa, Phys. Status Solidi A **19**, 707 (1983).
[18]P. K. Leung and J. C. Wright, Philos. Mag. **30**, 185 (1974).
[19]K. Kimura and F. Yonezawa, in *Topological Disorder in Condensed Matter,* edited by F. Yonezawa and T. Ninomiya (Springer, Berlin, 1983).
[20]H. Rudin, S. Jost, and H.-J. Güntherodt, J. Non-Cryst. Solids **61&62**, 291 (1984).
[21]A. Defrain, L. Bosio, R. Cortes, and P. G. Da Costa, J. Non-Cryst. Solids **61&62**, 439 (1984).
[22]D. Shechtman (private communication).
[23]F. C. Frank and J. S. Kasper, Acta Crystallogr. **11**, 184 (1958); **12**, 483 (1959).
[24]For a Frank-Kasper phase with an infinite unit cell, see R. Mosseri and J. F. Sadoc, J. Phys. (Paris) Lett. **45**, L827 (1984).
[25]This observation is due to C. Henley.
[26]D. R. Nelson and S. Sachdev, Phys. Rev. B **32**, 689 (1985).
[27]J. Hafner, Phys. Rev. B **21**, 406 (1980).
[28]T. V. Ramakrishnan and M. Yussouff, Phys. Rev. B **19**, 2775 (1979).
[29]S. Alexander and J. P. McTague, Phys. Rev. Lett. **41**, 702 (1978).
[30]P. Bak, Phys. Rev. Lett. **54**, 1517 (1985); Phys. Rev. B (to be published); in *Scaling Phenomena in Disordered Systems,* edited by R. Pynn and A. Skjeltrop (Plenum, New York, in press).
[31]N. D. Mermin and S. M. Troian, Phys. Rev. Lett. **54**, 1524 (1985).
[32]P. A. Kalugin, A. Yu Kitaev, and L. C. Levitov, Pis'ma Zh. Eksp. Teor. Fiz. **41**, 85 (1985) [JETP Lett. **41**, 119 (1985)].
[33]M. V. Jaric (unpublished).
[34]G. Baym, H. A. Bethe, and C. Pethick, Nucl. Phys. A **175**, 1165 (1971).

[35]D. Levine, T. C. Lubensky, S. Ostlund, S. Tamaswamy, P. J. Steinhardt, and J. Toner, Phys. Rev. Lett. **54**, 1520 (1985).
[36]T. V. Ramakrishnan, Phys. Rev. Lett. **48**, 541 (1982).
[37]A. D. J. Haymet and D. W. Oxtoby, J. Chem. Phys. **74**, 2559 (1981).
[38]D. W. Oxtoby and A. D. J. Haymet, J. Chem. Phys. **76**, 6262 (1982).
[39]A. D. J. Haymet, J. Chem. Phys. **78**, 4641 (1983).
[40]Y. Singh, J. P. Stoessel, and P. G. Wolynes, Phys. Rev. Lett. **54**, 1059 (1985); S. A. Rice, C. Cerjan, and B. Bagchi, J. Chem. Phys. **82**, 3350 (1985).
[41]See, e.g., A. J. M. Yang, P. D. Fleming, and J. H. Gibbs, J. Chem. Phys. **64**, 3732 (1976).
[42]P. Tarazon, Mol. Phys. **52**, 81 (1984); see also G. L. Jones and U. Mohanty, *ibid.* (to be published).
[43]R. Zallen, *The Physics of Amorphous Solids* (Wiley, New York, 1983).
[44]N. M. Korobov, Dokl. Akad. Nauk SSSR **115**, 1062 (1957).
[45]H. Conroy, J. Chem. Phys. **47**, 5307 (1967).
[46]P. A. Bancel, P. A. Heiney, P. W. Stephens, A. I. Goldman, and P. M. Horn, Phys. Rev. Lett. **54**, 2422 (1985).
[47]V. Elser and C. Henley (unpublished).
[48]R. J. Schaefer, W. J. Boettinger, F. S. Biancaniello, and D. Shechtman in *Particle Searches and Discoveries—1976 (Vanderbilt Conference)*, Proceedings of the Second International Conference in High Energy Physics at Vanderbilt University, edited by R. S. Panvini (AIP, New York, 1976) (AIP Conf. Proc. No. 30).
[49]B. P. Albles, C. Van der Marel, W. Geertsma, J. A. Meijer, A. B. Van Oosten, J. Dijkstra, P. C. Stein, and W. Van der Lugt, J. Non-Cryst. Solids **61&62**, 201 (1984).
[50]D. A. McQuarrie, *Statistical Mechanics* (Harper and Row, New York, 1976), p. 90.
[51]D. S. Boudreaux and J. M. Gregor, J. Appl. Phys. **48**, 152 (1977).
[52]A. D. J. Haymet (private communication).
[53]S. J. Poon, A. J. Drehman, and K. R. Lawless (unpublished).